Steel and Composite Structures, *Vol. 38, No. 4 (2021) 399-414*
DOI: https://doi.org/10.12989/scs.2021.38.4.399

Research on shear distribution of perfobond connector groups with rubber rings

Yangqing Liu[1a], Haohui Xin[1,2b] and Yuqing Liu*[1,]

[1]*Department of Bridge Engineering, Tongji University, Shanghai, China*
[2]*Faculty of Civil Engineering and Geosciences, Delft University of Technology, Netherlands*

(*Received July 16, 2019, Revised December 13, 2020, Accepted January 28, 2021*)

Abstract. This paper aims to verify the feasibility of rubber rings to mitigate the shear concentration in perfobond connector (PBL) groups. Firstly, modified push-out tests for five specimens with four holes were conducted to investigate the effects of rubber rings on the shear mechanism of PBL groups. The test results showed that by employing rubber rings on partial holes, more shear forces were distributed to the holes without rubber rings. The rubber rings significantly improved the slip ability of the specimens, and the ductility of PBL groups is dependent on the number and thickness of rubber rings. Subsequently, three-dimensional numerical models were established and validated by the experimental results. According to the plastic strain distribution in concrete dowels, the action principle of rubber rings in PBL groups was explained. Furthermore, the parametric study was conducted to investigate the influential factors on shear distributions, including the width of steel plates, the hole spacing, the number of holes, the rubber ring thickness, and the positions of rubber rings. The parametric analysis results showed that the redistribution of shear forces is significantly affected by the rubber rings with the smallest thickness. By properly employing rubber rings in PBL groups, the shear forces of holes are more even. Finally, an analytical model for PBL groups with rubber rings was proposed to predict the shear distribution at the serviceability stage.

Keywords: composite bridges; perfobond connector; rubber ring; modified push-out test; shear distribution

1. Introduction

Recently, perfobond connectors (PBLs) are increasingly applied in steel and concrete composite bridges due to their great shear capacity and fatigue resistance (Liu 2018). To transfer the huge load between steel and concrete components, PBLs are always in the arrangement with multiple rows and columns, such as the joints of composite beams (Hechler 2011), steel-concrete composite decks (Allahyari 2014), hybrid girder joints (Kim 2011), and anchorage joints between suspenders and girders (Liu 2018). Fig. 1 shows two types of PBL group in practices, including perfobond steel plates and perfobond ribs. The current design specifications assume that the shear distributions in shear connector groups are uniform and require that the number of shear connectors is no less than the total load divided by the design strength of a single connector. However, previous studies revealed that the shear distributions are uneven in both types of PBL groups particularly at serviceability stages (Oguejiofor 1994, Cândido-Martins 2010, Ahn 2010), and partial holes in PBL groups could be influenced by the local shear concentration, which will lead to an unsafe design.

Several researchers reported the uneven shear distribution in multiple PBLs by experimental studies. Oguejiofor (1994) conducted push-out tests for the specimens with different numbers of holes and concluded that the shear capacity of holes is affected by the adjacent holes. Ahn (2010) carried out push-out tests on the specimens with two ribs arranged side by side. The average shear capacity of the twin ribs decreased to 80% capacity of a single rib. Also, Liu (2018) investigated the shear distribution in multiple rows and columns of PBLs in suspender-girder composite anchorage joints. The PBLs with lower shear stiffness can distribute more loads to the middle and rear rows. The redistribution in shear requires the shear connectors to have sufficient ductility (Classen 2018). Based on these concepts, a new type of rubber-ring perfobond connector (RPBL) was proposed to alleviate the shear concentration in PBL groups (Liu 2019). Rubber rings can postpone the shear resistance of the critical PBLs in groups so that other PBL holes undertake more shear in the early loading stage. However, the feasibility of employing rubber rings to redistribute shear loads in PBL groups should be proved by experimental studies.

In addition to push-out tests, nonlinear finite element simulations provide a good alternative to investigate the inside failure modes and force distribution. (Kraus 1997, Nguyen 2009, Al-Darzi 2007, Pavlović 2013, Spremic 2017, Khorramian 2017, Kim 2019). Further parametric studies could save massive experimental costs and present the impacts of varibles on shear distribution. Besides, a practical and efficient expression to evaluate the uneven

*Corresponding author, Professor
E-mail: yql@tongji.edu.cn
[a]Ph.D.
E-mail: 1432232@tongji.edu.cn
[b]Ph.D.
E-mail: tjxinhaohui@gmail.com

ISSN: 1229-9367 (Print), 1598-6233 (Online)

Table 1 Parameters of specimens

Specimen	d (mm)	d_s (mm)	n	t_r (mm)	Pos.	V_y (kN)	s_y (mm)	V_u (kN)	s_u (mm)
MPB-1	60	20	4	-	-	1607.5	1.42	1839.8	19.08
MPB-2	60	20	4	4	1, 2, 3, 4	1091.1	6.50	1647.0	33.24
MPB-3	60	20	4	2	1 ,4	1437.1	3.46	1789.5	24.11
MPB-4	60	20	4	4	1, 4	1401.3	5.10	1711.7	22.11
MPB-5	60	20	4	6	1, 4	1436.8	7.77	1739.7	26.64

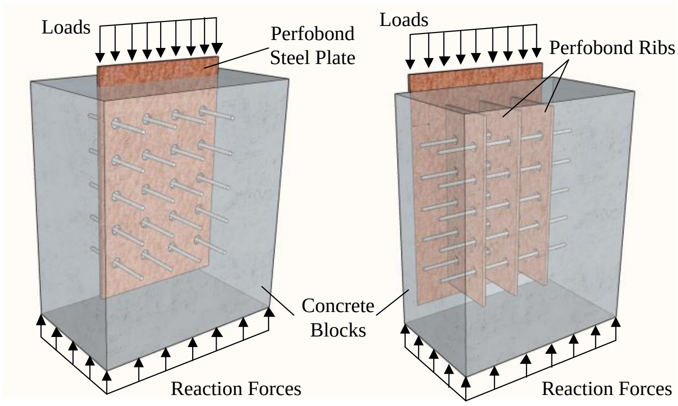

(a) Perfobond steel plates (b) Perfobond ribs

Fig. 1 Typical perfobond connector groups

shear distribution in multiple PBLs will be useful for design.

Therefore, this paper documents the modified push-out tests for five specimens with four holes conducted to investigate the effects of rubber rings on the shear mechanism of PBL groups. Based on the test results, the failure modes, the load-slip curves, and the load-strain curves of steel plates and perforated rebars were discussed. Subsequently, 3-D nonlinear FEA models were established and validated by the test results. The redistribution of shear forces was presented by the plastic strains in concrete dowels. Furthermore, the effects of perfobond plate widths, spacing and numbers of holes, rubber ring thicknesses, and positions of rubber rings on the shear distribution were investigated by the FEA parametric study. Finally, an analytical model for PBL groups with rubber rings was proposed to predict the shear distribution at the serviceability stage.

2. Modified push-out test

2.1 Test specimens

To validate the feasibility of improving shear distribution in PBL groups by partially setting rubber rings, the modified push-out tests for five specimens with four rows of holes were conducted. Table 1 and Fig. 2 show the specimen parameters and configuration. The hole diameter and center-to-center spacing are 60 mm and 200 mm, respectively. The diameters of the perforated rebars and distributed reinforcements are 20 mm and 16 mm, respectively.

Six triangle stiffeners were welded between the loading plate and the top surface of the concrete block to prevent the perfobond plates from buckling. Before the concrete casting, six plastic foams were placed below the corresponding stiffeners, and one woodblock was located under the perfobond plate. The woodblock was removed after curing and before loading. The configuration of rubber rings and the material properties of concrete, steel, and rubber are the same as the previous series of tests (Liu 2019).

2.2 Test Setup and Instrumentation

Fig. 3 shows the test setup and instrumentation. The servo-hydraulic machine used in the tests has a loading capacity of 20000 kN. Eight LVDTs with 1/1000 mm precision were positioned between the concrete blocks and the steel plates. Ahead of the loading, a lime layer with the thickness of 2 mm was paved on the top steel plate to keep the reaction force uniform. Subsequently, the preloading steps with the load range from 5% to 40% of the estimated ultimate capacity were performed, according to EUROCODE 4 (2005), followed by the formal monotonic loading controlled by displacement. The loading speed was 0.2 mm/min.

Five strain gauges were mounted along the steel plate cross-section above each hole. Meanwhile five strain gauges were used on each perforated rebar, as shown in Fig.

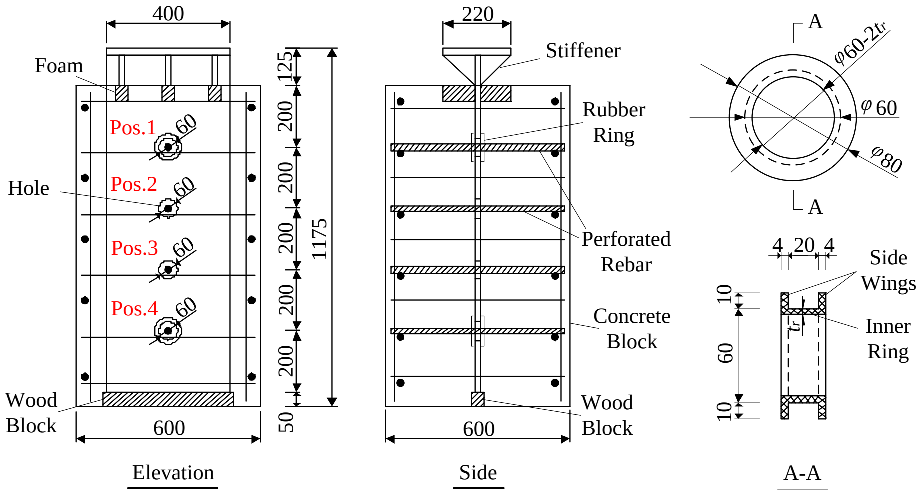

Fig. 2 Specimen configuration. (mm)

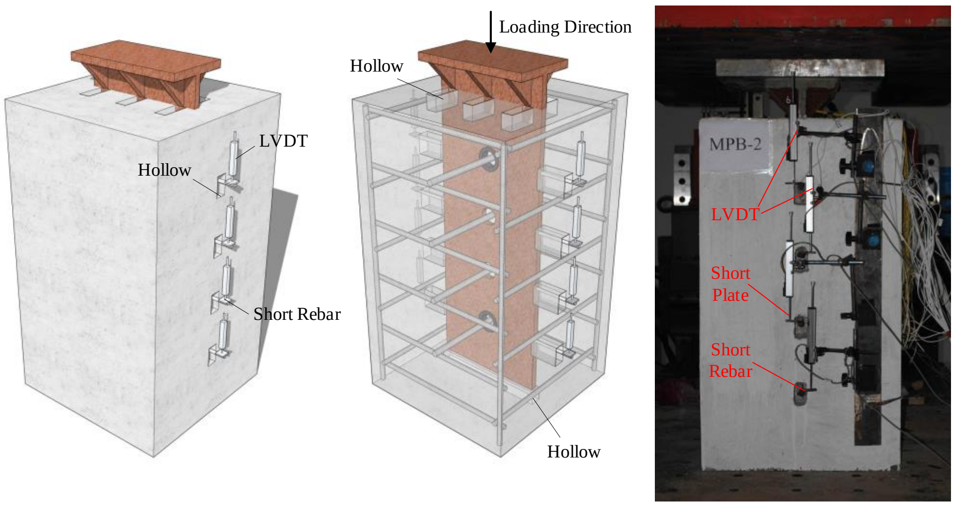

Fig. 3 Test setup and instrumentation

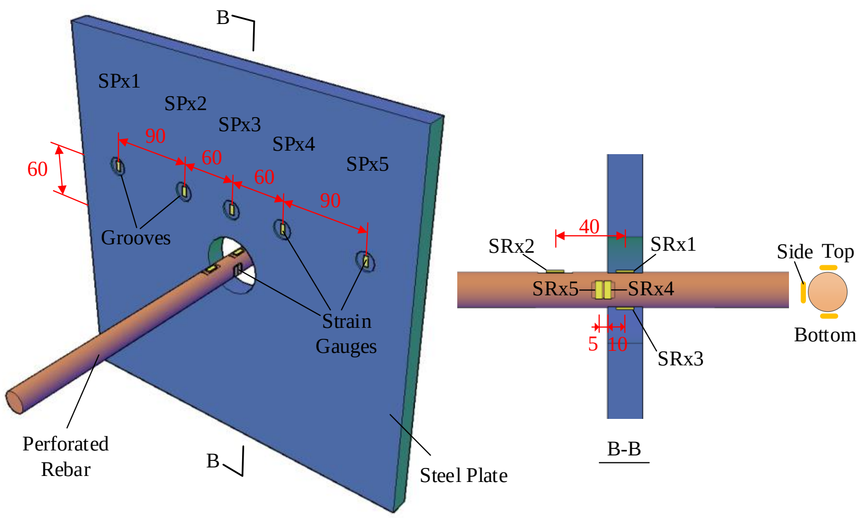

Fig. 4 Strain gauges on perfobond plates and perforated rebars. (mm)

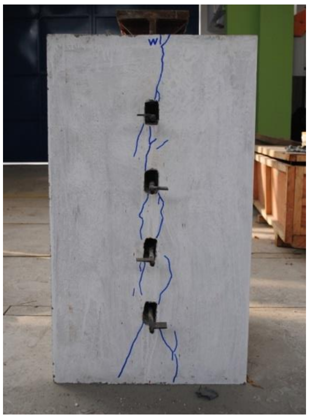

Fig. 5 Cracks on concrete blocks

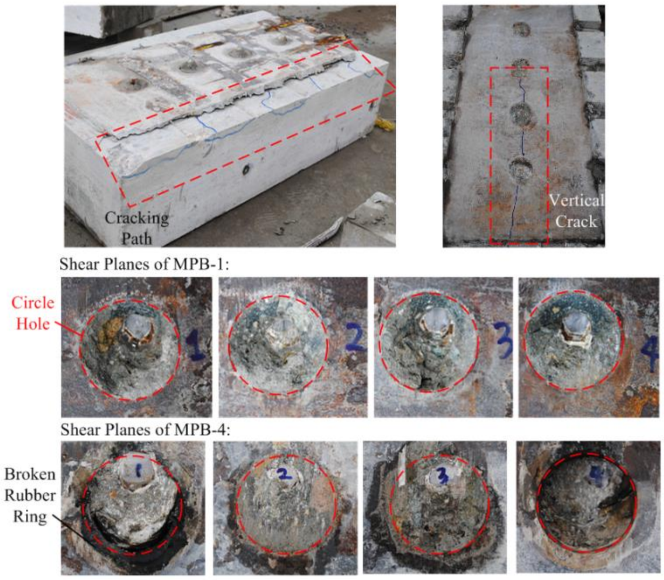

Fig. 6 Internal failure modes

4. The horizontal cross sections for mounting strain gauges were 60 mm from the center of holes. Grooves with 2 mm depth and 20 mm diameter were set on steel plates to protect the strain gauges from damage. As for the strain gauges on the perforated rebars, three of them were parallel to the longitudinal direction of rebars, while the other two were perpendicularly arranged on the side. In the figure, the letter "x" denoted the number of holes. For example, "SP23" represented the third strain gauge above the second hole on the steel plate.

3. Test results

3.1 Failure modes

Fig. 5 shows the crack distribution on concrete blocks after loading. The cracking mainly occurred on the side surfaces perpendicular to the perfobond plate and the top surface, while no cracks were found on the side surfaces parallel to the perfobond plate. Most of the cracks on the side surfaces were along the edges of the perfobond plates. Besides, the cracks on the top surface started from the perfobond plate and ended to the side surfaces. After the failure of specimens, the concrete blocks were separated into two parts by cutting along the perfobond plate edges.

Fig. 6 displays the internal failure modes of concrete blocks. There were four prime horizontal cracks near the height of four holes extending to the side surfaces. The vertical cracking was also observed between adjacent holes except for the first two holes. The reason is that the total force in the cross-section of concrete increases with depth. However, these vertical cracks did not develop to the surfaces parallel to the perfobond plate. As for the failure of concrete dowels, the shear fracture planes formed along the surfaces of the perfobond plate. The upper regions of

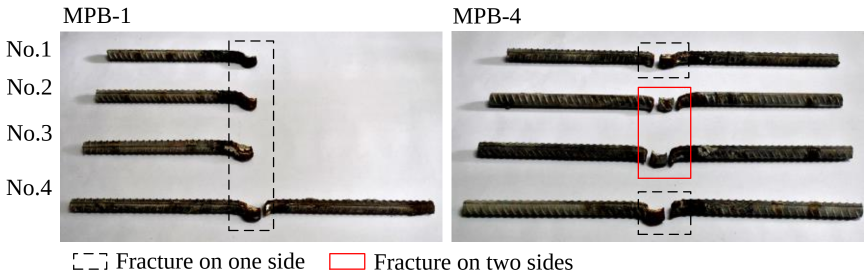

Fig. 7 Fracture characters of perforated rebars

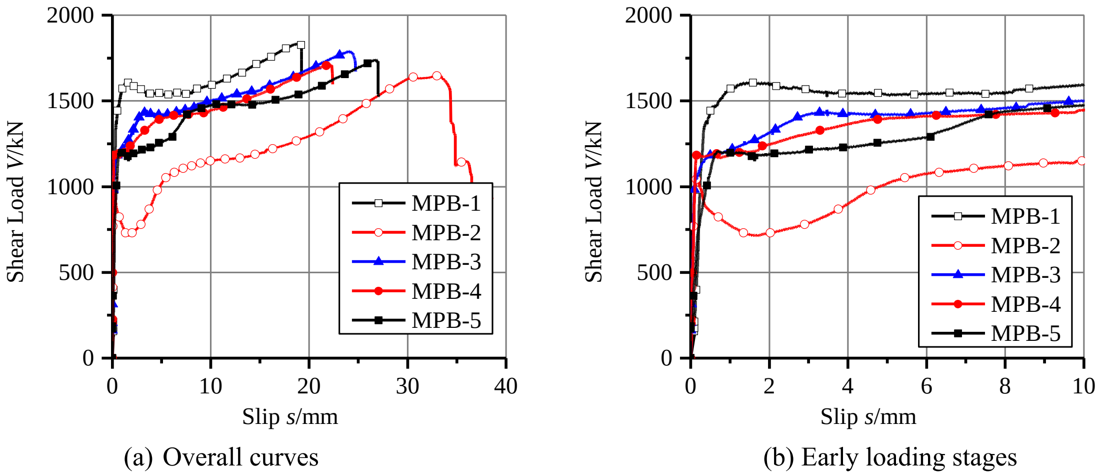

Fig. 8 Shear force – slip curves

concrete dowels were always compacted, and the rubber rings close to the loading side were utterly squashed. The nearby parts of side wings suffered from large shear deformation and were sheared off.

When the applied load increased to the ultimate shear capacity, distinct fracture sounds of perforated rebars were heard one by one. Subsequently, the sheared off rebar were taken out from the concrete blocks, as shown in Fig. 7. All the perforated rebars in MPB-1 only had one fracture plane. The second and third perforated rebars in MPB-4 had two fracture planes, indicating that the holes at the second and the third row undertook more loads and were fully utilized in the PBL groups. The shear forces were successfully distributed to the middle holes.

3.2 Load-slip curves

In the following discussion, the yield load V_y and the yield slip s_y are defined as the first local peak shear force and the corresponding slip on the curves. Besides, the shear capacity V_u and ultimate slip s_u represent the ultimate shear force and slip leading to the failure of specimens. The test results summarized in Table 1 illustrate that the rubber rings increased the deformation ability of multi-row PBLs. Both the yield slip and the ultimate slip increased with the number and thickness of rubber rings. Due to the reduction of confinement effects on concrete dowels, the yield loads of MPB-3, MPB-4, and MPB-5 were respectively 11%, 13% and 11% smaller than that of MPB-1. However, setting rubber rings had less influence on the shear capacity. The reason is that the ultimate load was dominated by ductile fracture of perforated rebars.

Fig. 8 shows the load-slip curves of the specimens, where the slips equal the mean value of LVDTs in the first row. The load-slip curves generally consist of three stages, including the initial linear stage with high stiffness, the plastic stage with decreasing stiffness and the hardening stage ended by the shear fractures of perforated rebars. In the first stage, the loads were primarily resisted by the bond force and the concrete dowels without rubber rings. After the damage of bond, the loads were taken by the concrete dowels and the perforated rebars. The overall stiffness of the second stage decreased with the thickness of rubber rings. The stiffness recovered at a smaller slip in the cases with thinner rubber rings. As the slips grew further, the shear planes formed and the perforated rebars fell into the hardening stage, so that the loads approximately linearly rose to the ultimate capacity V_u.

3.3 Shear load-strain relationship on perfobond plate

Fig. 9 shows the shear load-strain relationships on the perfobond plates. The discussions mainly focus on the early loading stage since most of the gauges damaged when slip

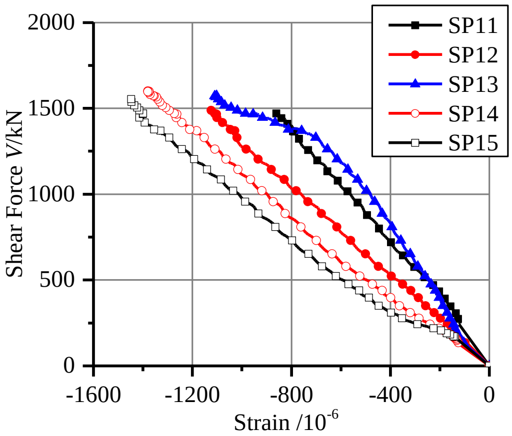

(a) 1st row of MPB-1

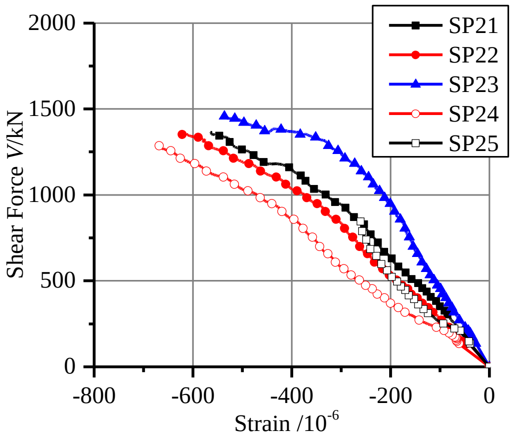

(b) 2nd row of MPB-1

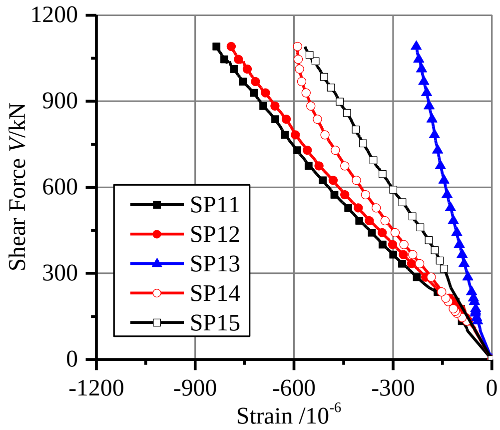

(c) 1st row of MPB-3

Fig. 9 Load – strain relationship on steel plates

rapidly increased. Overall, the strains on steel plates linearly grew with the shear loads except the strains at SPx3 in MPB-1. Due to the bond forces between perfobond plates and concrete blocks, the strains at the centerline of the steel plate (SPx3) were minimal. Subsequently, the concrete dowel started to undertake shear forces as the load increased, so that the compressive strains above circle holes significantly rose, as shown in Figs. 9(a) and 9(b). However, the shear resistance of the first concrete dowel in MPB-3 was postponed by setting rubber rings. Thus, the shear load-strain relationship at SP13 kept linear, as presented in Fig. 9 (c).

Fig. 10 compares the average strains on the perfobond plates at different rows in MPB-1 and MPB-3, where the curves are labeled by the specimen number and the row number (i.e., “MPB-a-b” denotes the bth row in specimen MPB-a). Overall, the strains decreased with the row numbers, and the shear load–strain relationship was approximately linear at each row. It is found that by employing a rubber ring on the first hole, the slope difference between the curves of the first two rows in MPB-3 was less than that in MPB-1. It reflected that the shear force resisted by the first hole decreased after setting the rubber ring. On the contrary, that rubber ring arrangement enlarged the shear force of the second hole.

3.4 Shear load-strain relationship on perforated rebars

Fig. 11 compares the longitudinal and vertical strains of the first perforated rebar in MPB-1 and MPB-3, where the number in brackets denotes the specimen label. Since the bond forces resisted parts of the shear loads, the longitudinal strains on perforated rebars were relatively small at the early loading stage, as shown in Fig. 11(a). However, the strains increased rapidly after the bond damage occurred. The longitudinal strains of the first perforated rebars in MPB-3 were smaller than those in MPB-1. The reason is that the rubber ring reduced the contribution of the concrete dowel on the shear force. Fig. 11(b) shows the strains perpendicular to perforated rebars near the shear planes. At the early loading stage, the vertical rebar strains were small and in tension. Then they turned to compressive strains and significantly increased with the growth of loads, indicating that the rebars presented primary bending or shear behavior at different loading stages. Fig. 12 shows the longitudinal strains on the bottom edges of perforated rebars in different rows. The strain at the first row was maximal among all the four perforated rebars in MPB-1, while the second rebar had the most substantial strain in MPB-3. That once again demonstrated that the rubber rings were effective to delay the shear force.

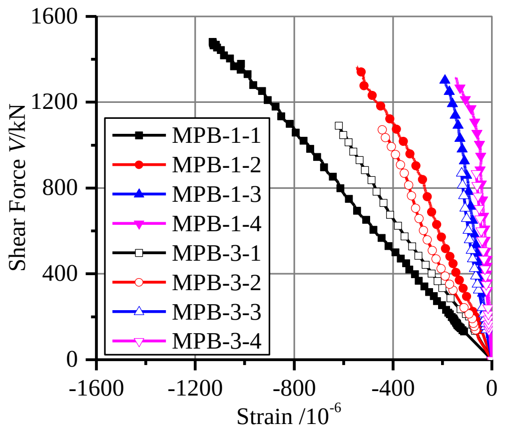

Fig. 10 Comparison of strain distribution

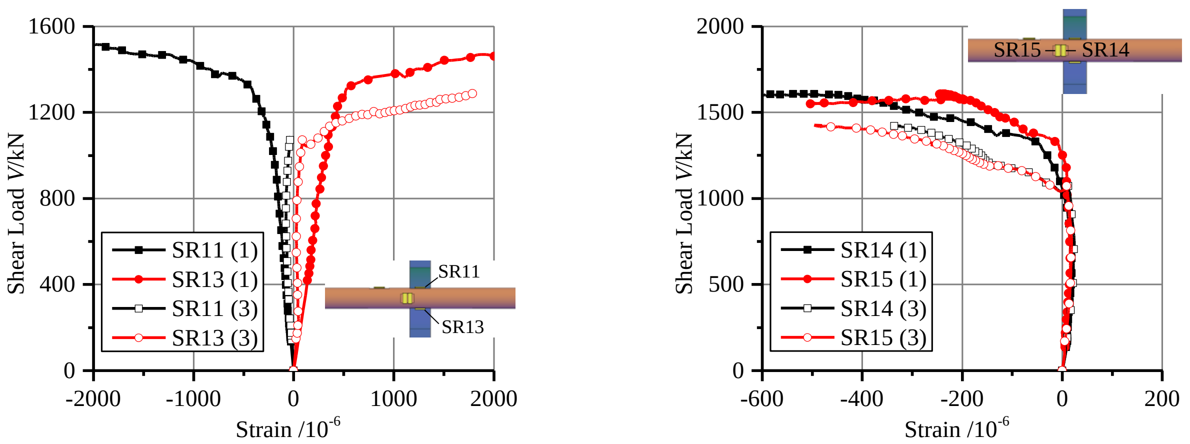

(a) Longitudinal strain (b) Vertical strain

Fig. 11 Comparison of perforated rebar strains

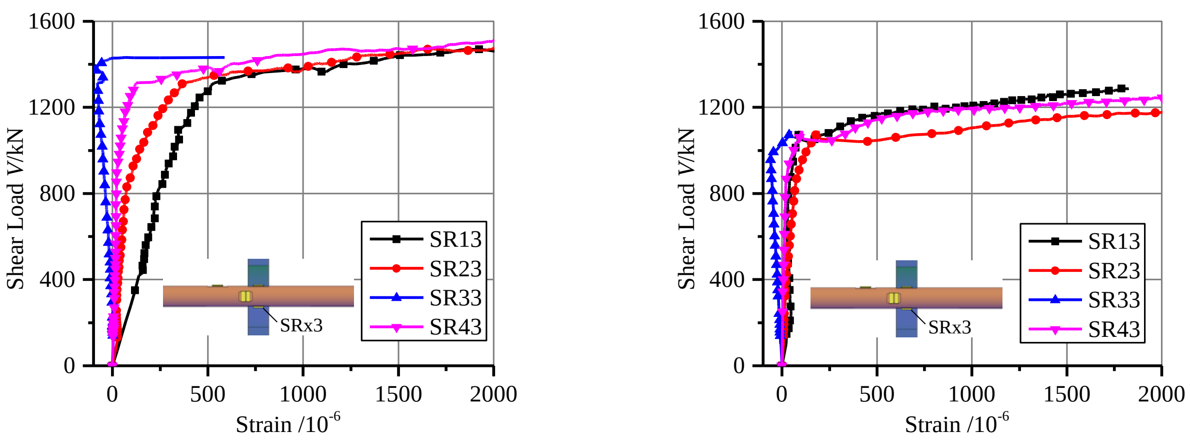

(a) MPB-1 (b) MPB-3

Fig. 12 Perforated rebar strains in different rows

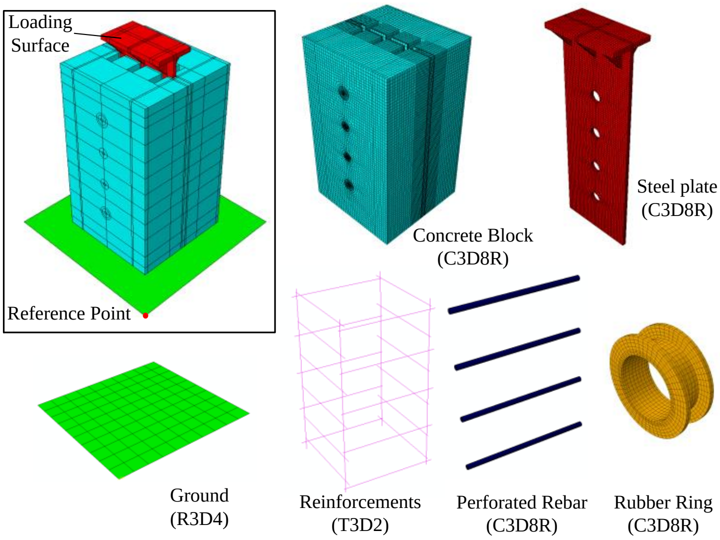

Fig. 13 Finite element model of multi-PBL

4. Finite element analysis

4.1 Finite element model

The three-dimensional multi-hole models were built by ABAQUS / Explicit [17] to investigate the effects of rubber rings in PBL groups. The models consist of the perfobond plates, perforated rebars, rubber rings, concrete blocks, distributed reinforcements, and rigid grounds. Fig. 13 shows the geometry shape of the model and the element types used for each part. The boundary condition is consistent with that in the lab test. The modeling method, including the material modeling of concrete, steel, and rubber, and the interface properties, refers to the previous work (Liu 2019, CEB-FIP MC2010, Zheng 2016).

4.2 Model validation

Fig. 14 compares the shear load-slip curves from the finite element (FE) models with those from the tests. Overall, the numerical works can properly predict the yield shear loads and shear capacities of the PBL groups. The entire failure process of the experimental specimens, including the three stages above is successfully simulated by the FE models. Note that in the hardening stage, the stiffness of the models are higher than those of the test specimens. The ductile damage of the perforated rebars should be introduced in future studies.

Moreover, the strains on the perfobond plates of the models with or without rubber rings were compared to the corresponding test results, as shown in Fig. 15. The trends of the shear load-strain relationship from the tests and FE models agreed well, indicating the modelling is valid to perform further analyses and discussions.

4.3 Shear mechanism

Fig. 16 shows the plastic principal compressive strains of the concrete dowels in the models with or without rubber rings. The X-shape region at the upper part of concrete dowels has the maximum principal compressive strains. Because of the confinement effects provided by perforated rebars and surrounding concrete, the concrete is under the complex multi-axial stress state. The shear planes show up between the corner points in concrete dowels under the yield shear load.

Column (a) presents the results from model MPB-1 at the yield shear load V_y. The plastic compressive strains in the different holes decrease from top to bottom, indicating that the first hole undertook more shear forces than the average shear load. Secondly, Column (b) shows the plastic strain distribution in model MPB-3 under the same slip as model MPB-1. The rubber rings postpone the shear resistance of the first and the fourth holes so that these two concrete dowels are in the elastic state. As the slip increases, the plastic strains of the concrete dowels when the shear loads approach the yield shear load are shown in Column (c). By employing rubber rings on the top and bottom holes, the shear strength of holes in the middle rows can be sufficiently exerted. Based on the numerical results above, it is found that setting a rubber ring on the bottom hole is unnecessary in a perfobond connector group with four holes and a large concrete cross-section. The thickness of rubber rings smaller than 2 mm is more useful in practice. Furthermore, the parametric study performed to investigate the effects of rubber rings and plate dimensions on the shear distribution is presented in the next section.

4.4 Parameter analysis

The parameter study is performed to investigate the shear distributions and verify the effectivity of rubber rings in PBL groups. Based on the modeling methodology above, a total of 17 multi-hole PBL models with varying steel plate widths, hole spacing, hole numbers, rubber ring thicknesses and schemes are established, as shown in Table 2. Wherein,

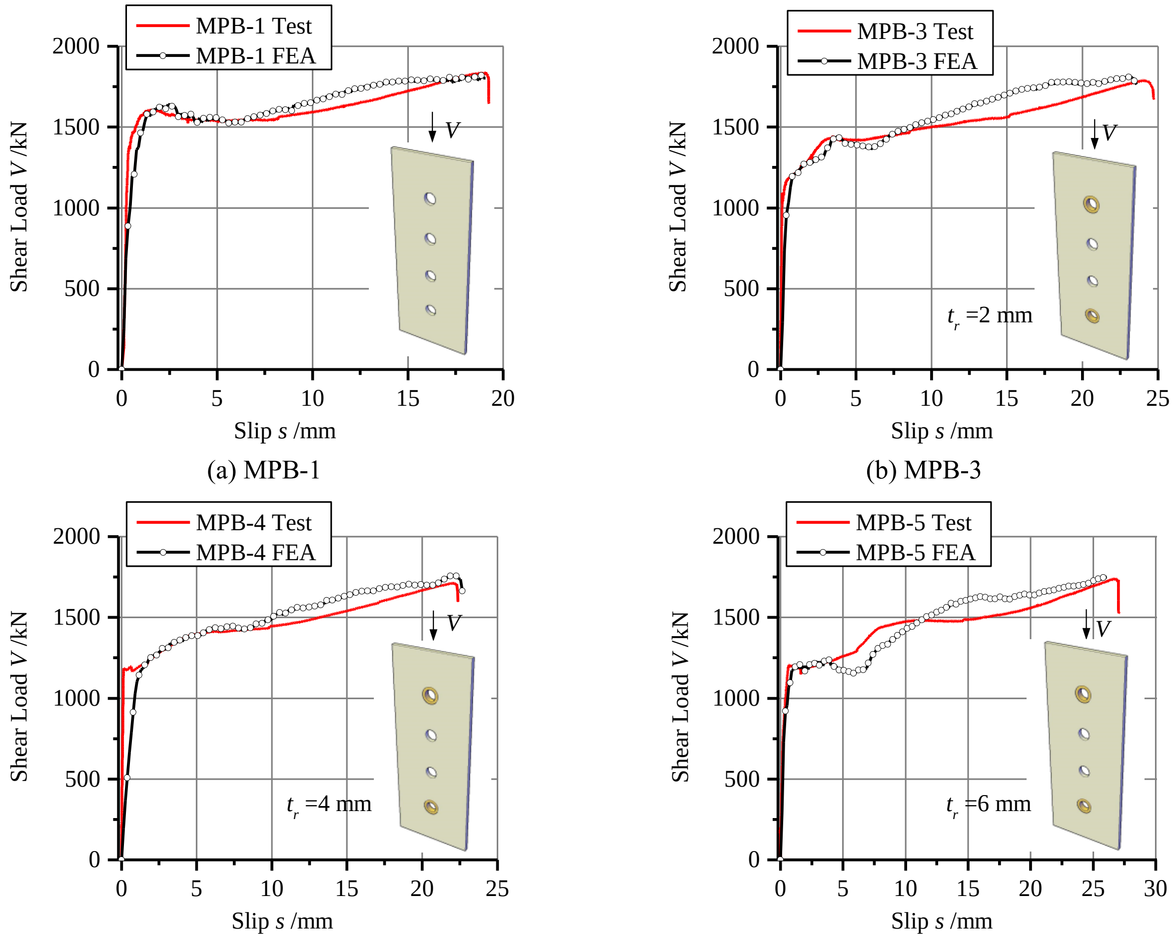

(a) MPB-1 (b) MPB-3

(c) MPB-4 (d) MPB-5

Fig. 14 Comparison of shear force - slip curves

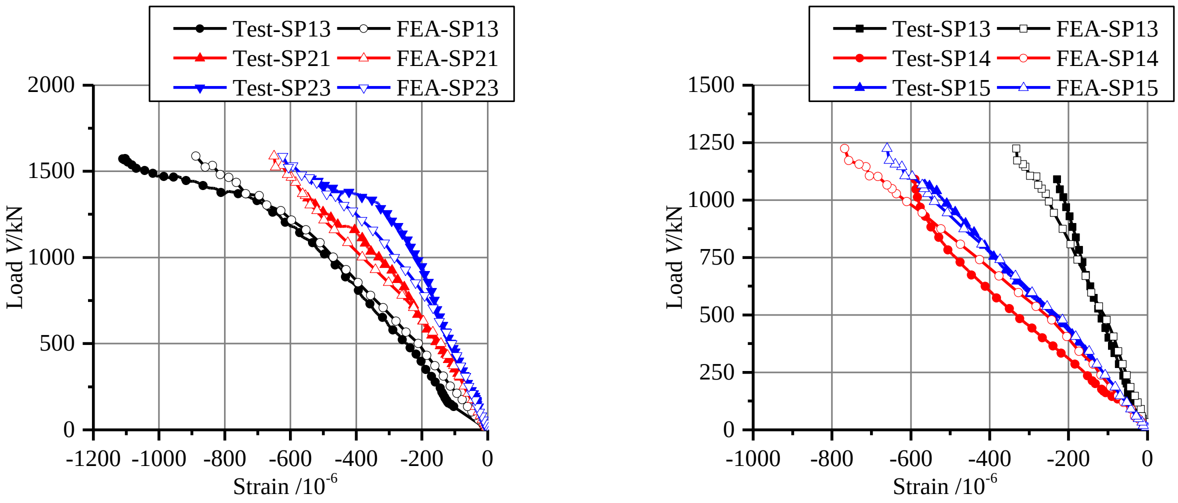

(a) MPB-1 (b) MPB-3

Fig. 15 Comparison of strains on perfobond plates

n, w, a, t_r denote the hole numbers, the steel plate width, the longitudinal center-to-center spacing of adjacent holes and the rubber ring thickness respectively. The typical spacing in applications is 200 mm for the PBLs with 60 mm diameter (Ahn 2010, Su 2014, Wang 2019, Zhang 2017) so that the reference width and hole spacing are set to 200 mm

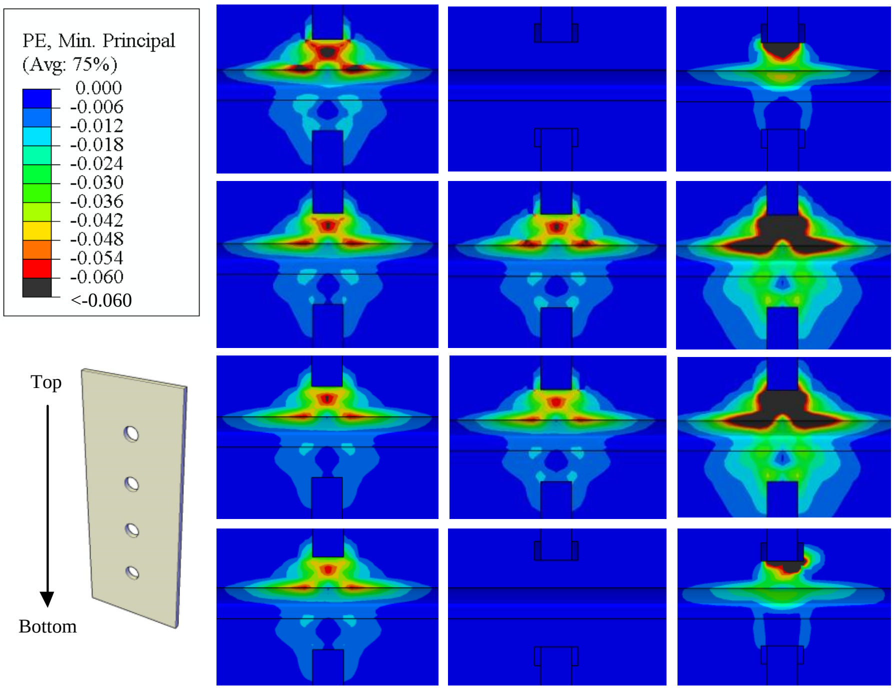

(a) MPB-1 ($V_{y,\,\mathrm{MPB\text{-}1}}$) (b) MPB-3 ($s_{y,\,\mathrm{MPB\text{-}1}}$) (c) MPB-3 ($V_{y,\,\mathrm{MPB\text{-}3}}$)

Fig. 16 Plastic strains of concrete dowels

Table 2 Investigated models in parametric study

No.	Model	n	*w* /mm	*a* /mm	Pos.	t_r /mm	Parameter
1	n4-w150	4	150	200	-	-	Width
2	n4-w200	4	200	200	-	-	
3	n4-w250	4	250	200	-	-	
4	n4-w300	4	300	200	-	-	
5	n4-w400	4	400	200	-	-	
6	n4-a150	4	200	150	-	-	Hole spacing
7	n4-a250	4	200	250	-	-	
8	n4-a300	4	200	300	-	-	
9	n4-a400	4	200	400	-	-	
10	n4-p1-tr1	4	200	200	1	1	Thickness
11	n4-p1-tr05	4	200	200	1	0.5	
12	n6	6	200	200	-	-	Number of holes
13	n8	8	200	200	-	-	
14	n10	10	200	200	-	-	
15	n6-p1-tr1	6	200	200	1	1	Scheme
16	n6-p12-tr05	6	200	200	1 & 2	0.5	
17	n6-p12-tr1_05	6	200	200	1 & 2	1 & 0.5	

in the simulations. The models are denoted by the investigated parameters. For example, Model n6-tr1-p1 represents a model with six holes and a 1 mm thick rubber ring on the first hole.

Fig. 17 shows the shear force distributions during the loading process in the six representative models, where the x-axis is the ratio of the total shear force to the yield shear load. Overall, the shear distribution tends to be more even with the increase of the total shear load, which is consistent with the previous experimental results. The reason is that the shear stiffness of partial holes decrease with the loading so that the stiffness ratio of the holes to the perfobond plates

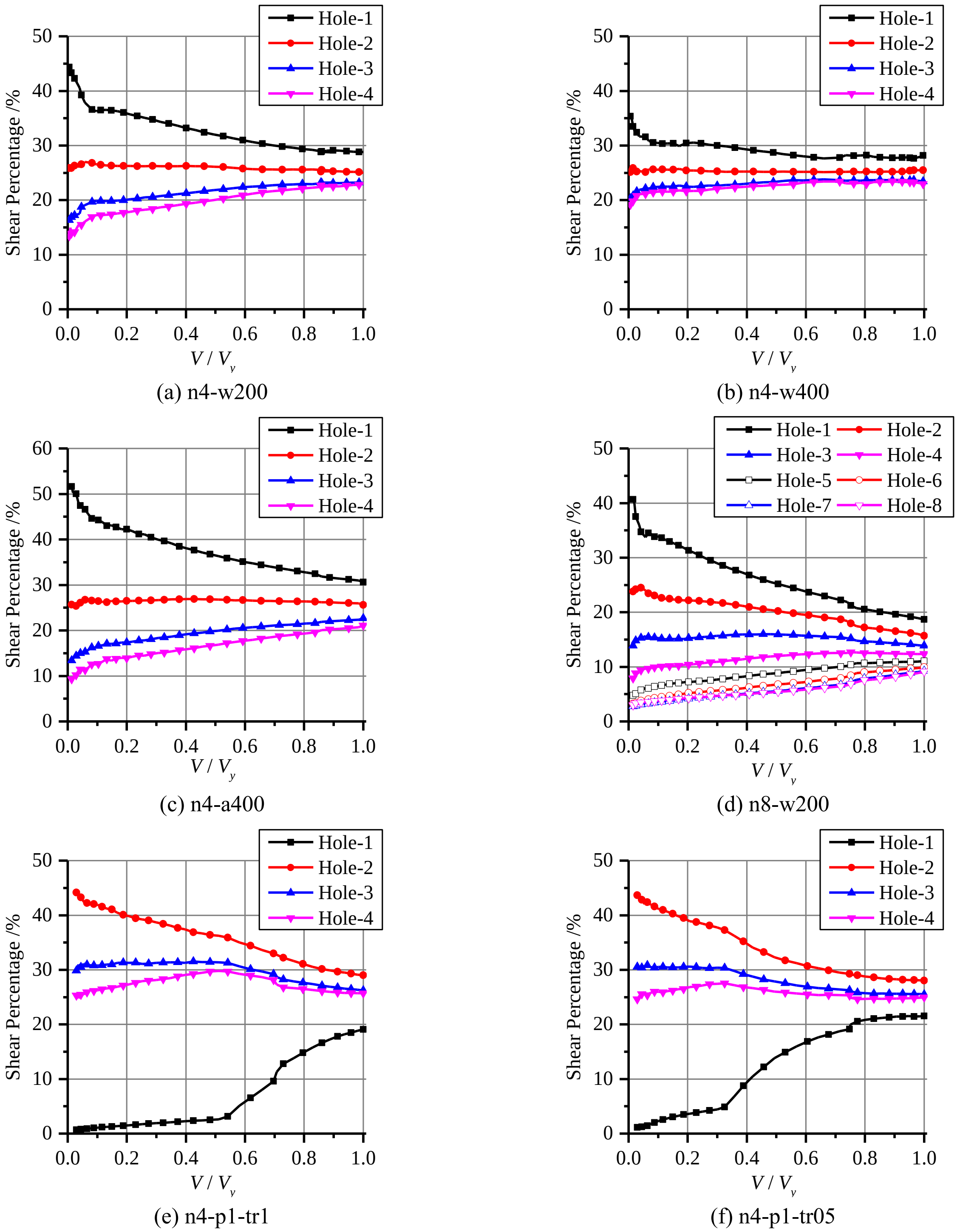

Fig. 17 Various effects on shear distributions

reduces. Figs. 17(a) and 17(b) shows the effects of plate widths on the shear distribution. According to the concept of the stiffness ratio above, the unevenness of the shear forces dropped by increasing the cross-section area of perfobond plates, i.e., the stiffness of perfobond plates. Likewise, the first hole undertakes more loads when the longitudinal hole spacing is enlarged from 200 mm to 400 mm, resulting from the smaller plate stiffness and the larger stiffness ratio, as shown in Figs. 17(a) and 17(c).

Fig. 17(d) displays the shear distribution in the model with eight rows of holes. It is found that the first two holes resist much higher shear forces than the average loads. The difference in the shear percentages of the first hole and the holes in the rear rows is huge. Compared with the four-hole model, the shear percentage of the first hole is close, thus the shear unevenness increases with the number of holes. Furthermore, Figs. 17(a), 17(e), and 17(f) present the results of models without and with a rubber ring on the first hole to

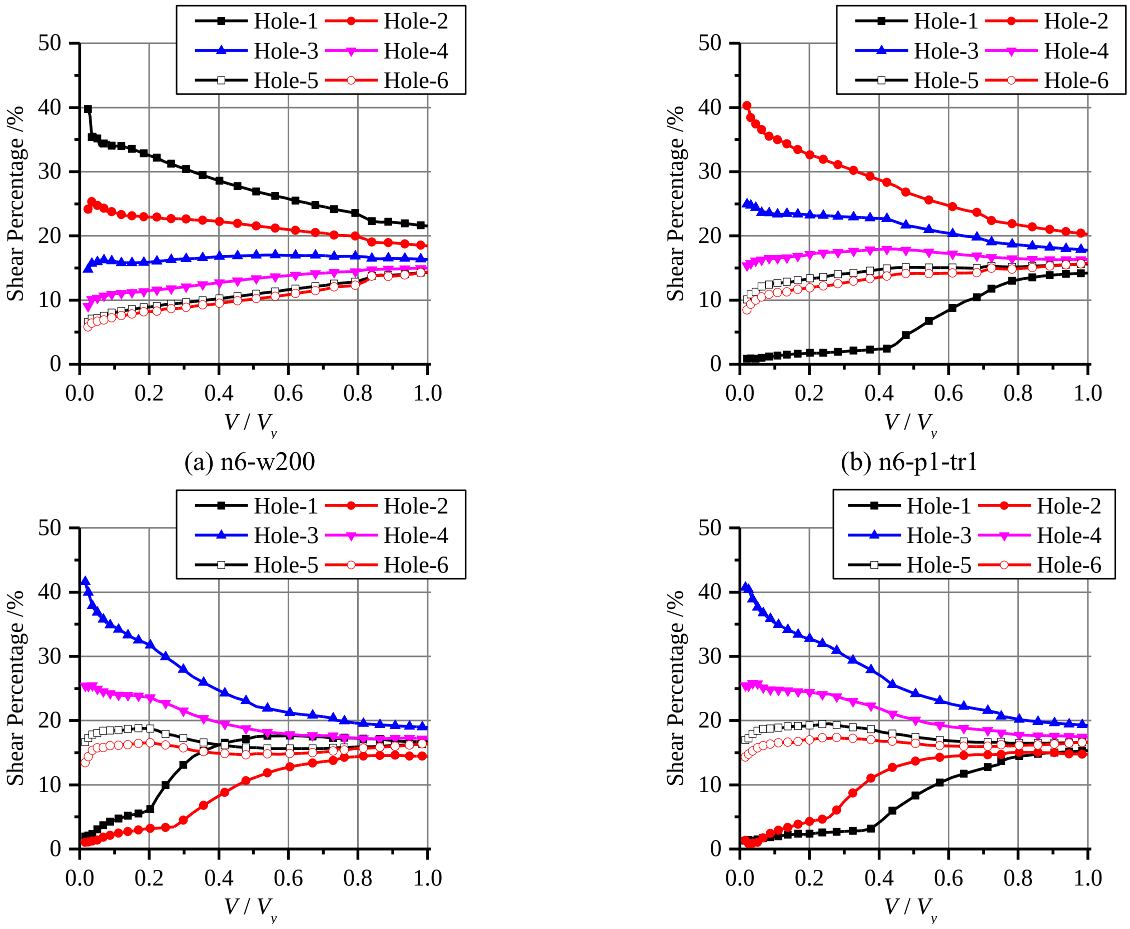

(a) n6-w200 (b) n6-p1-tr1

(c) n6-p12-tr05 (d) n6-p12-tr1_05

Fig. 18 Effect of rubber ring schemes on shear distributions

reflect the effects of rubber ring thickness on the shear distribution. The hole with a thicker rubber ring holds a small shear percentage at the early loading stage, and participates fully in undertaking the shear load at a larger slip. Therefore, employing rubber rings on the critical holes in PBL groups can protect the holes that suffer from shear concentration. When the shear stiffness of the rubber-ring holes recover with the increase of slips, the shear percentages of the holes without rubber rings drop rapidly, indicating the shear redistribution occurs in the PBL groups.

Fig. 18 shows the effects of rubber ring schemes on the shear distribution by the representative 6-hole models. The results above showed that the reasonable rubber ring thickness should be 1 mm and 0.5 mm. Since the shear force taken by the last hole was relatively small under the current dimensions, the rubber rings are arranged at the first one or two holes instead of the last hole. Fig. 18(b) shows the results of the model with a 1 mm thick rubber ring on the first hole. By employing the rubber ring, the shear percentages of the holes in the middle and rear rows rise, indicating that these holes are more efficiently configured. Besides, this rubber ring scheme achieves that the first hole resists the minor shear force at the beginning, and then undertakes approximate 1/6 of the total shear load with the increase of the applied load. However, the second hole undertakes considerable shear forces in the early loading stage, which should be optimized.

Fig. 18(c) displays the shear force distribution of the model with two 0.5 mm thick rubber rings on the first two holes. Compared with the model configuring a 1 mm thick rubber ring on the first hole, the force percentage of the first hole without rubber rings (the third hole) reduces faster with the increase of shear loads. That is caused by the smaller rubber ring thickness. Between the two holes with rubber rings, the stiffness recovery and the shear percentage of the first hole are earlier and higher than those of the second hole, resulting from the larger slip at the first hole. It is noted that the shear distribution when the shear load is over 60% of the yield shear load is more even than that in Fig. 18(a). Finally, Fig. 18(d) shows the results of the scheme using rubber rings with two different thicknesses. Since the rubber ring on the second hole is thinner, the shear percentage of the second holes is larger than that of the first hole. Besides, the shear force distribution of the holes without rubber rings is close to the distribution in Fig. 18(c), indicating that the shear force distribution is mainly controlled by the smallest thickness of rubber rings in the PBL groups. Consequently, reasonable arrangements of rubber rings can improve the shear distribution of PBL groups.

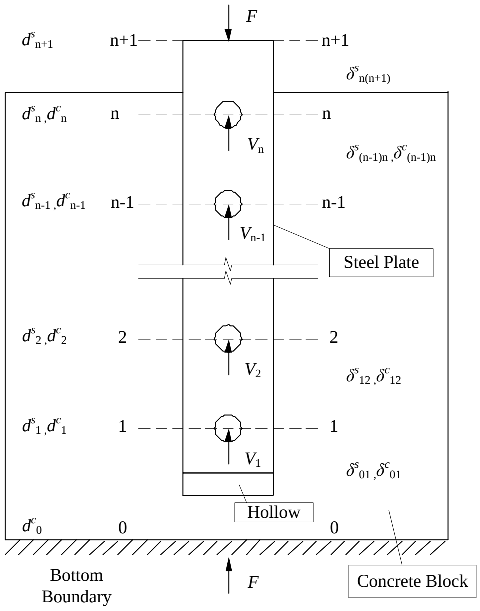

Fig. 19 Simplified mechanics model of multi-PBLs

5. Theoretical analysis on shear distribution

5.1 Mechanics model

In this section, an analytical model for multi-row shear connectors is proposed. Compared to the previous works by Liu (2018), the reaction force at the bottom boundary of concrete blocks and the deformation of concrete are taken into account. By considering the effects of concrete deformation, the shear distribution could be saddle-like, as reported in the previous studies (Zhang 2016). Besides, holes with different shear stiffness (i.e., partially employing rubber rings) are allowable in the analysis. Fig. 19 shows the simplified mechanics model of multi-row PBLs. The following assumptions are claimed by considering practical applications.

- The PBLs, steel plate and concrete block are in the elastic state.
- The spacing between adjacent holes is identical.
- The end bearing effect of the steel plate is neglected.

Based on the simplified mechanics model, the vertical equilibrium equation is given as Eq. (1), where V_i is the shear force of the i^th^ hole from bottom to top (kN); F is the total load applied on the top surface of the steel plate (kN). Since the displacement of one hole equals to the sum of the displacement at the previous hole and the elastic deformation of the steel plate (the concrete block) between the two adjacent holes, the deformation compatibility equations are established as Eqs. (2) and (3)

$$\sum_{i=1}^{n} V_i - F = 0 \tag{1}$$

$$d_i^s + \delta_{i(i+1)}^s = d_{i+1}^s, \quad i = 1 \cdots n \tag{2}$$

$$d_i^c + \delta_{i(i+1)}^c = d_{i+1}^c, \quad i = 0 \cdots n-1 \tag{3}$$

Where d^s_i and d^c_i are the displacements of steel plates and concrete blocks at the i^{th} hole (mm); $\delta^s_{i(i+1)}$ and $\delta^c_{i(i+1)}$ are the deformation of steel plates and concrete blocks between the i^{th} and $(i+1)^{th}$ cross-sections (mm). s_i represents the slip of i^{th} hole (mm), which equals the difference between d^s_i and d^c_i. The constitutive equations for perfobond connectors, steel plates and concrete blocks are defined as Eqs. (5)-(7)

$$s_i = d_i^s - d_i^c \tag{4}$$

$$V_i = k_{pi} s_i, \quad i = 1 \cdots n \tag{5}$$

$$k_s \delta_{i(i+1)}^s = \sum_{j=1}^{i} V_j, \quad i = 1 \cdots n \tag{6}$$

$$k_c \delta_{i(i+1)}^c = \sum_{j=i+1}^{n} V_j, \quad i = 0 \cdots n-1 \tag{7}$$

Where k_{pi} is the shear stiffness of the i^{th} hole ($kN \cdot mm^{-1}$); k_s is the axial stiffness of the steel plate ($kN \cdot mm^{-1}$); k_c is the axial stiffness of concrete block ($kN \cdot mm^{-1}$). If all the holes have the same stiffness (i.e., $k_{pi} = k_p$), the following equations can be obtained by Eqs. (2) to (7)

$$d_i^s + \frac{k_p}{k_s} \sum_{j=1}^{i} s_j = d_{i+1}^s, \quad i = 1 \cdots n \tag{8}$$

$$d_i^c + \frac{k_p}{k_c} \sum_{j=i}^{n} s_j = d_{i+1}^c, \quad i = 0 \cdots n-1 \tag{9}$$

To simplify the derivation process, the stiffness ratios of PBL to steel plates and PBL to concrete blocks are defined as ξ_s and ξ_c, respectively. The sum of them denotes as ξ. By substituting Eq. (10) into the difference between Eqs. (8) and (9), the slip relationship Eq. (11) can be written as

$$\frac{k_p}{k_s} = \xi_s, \quad \frac{k_p}{k_c} = \xi_c, \quad \xi = \xi_s + \xi_c \tag{10}$$

$$s_i + \xi_s \sum_{j=1}^{i} s_j - \xi_c \sum_{j=i+1}^{n} s_j = s_{i+1}, \quad i = 1 \cdots n-1 \tag{11}$$

Through Eq. (11), when i > 2 the recursive formula of s_i can be described as Eq. (12), and the general formula is solved by using the characteristic equation. Since ξ is greater than zero, the characteristic Eq. (13) has two different roots, x_1 and x_2. The general formula of s_i can be expressed as Eq. (14)

$$s_i - (2+\xi)s_{i-1} + s_{i-2} = 0, \quad i = 3 \cdots n \tag{12}$$

$$x^2 - (2+\xi)x + 1 = 0 \tag{13}$$

$$s_i = Ax_1^{i-1} + Bx_2^{i-1}, \quad i = 1 \cdots n \tag{14}$$

By solving the characteristic Eq. (13), the expressions of x_1 and x_2 are obtained. Noted that $d^c{}_1$ equals to F divided by k_c. By substituting the Eqs. (11) and (1) into Eq. (17), the expression of s_2 is simplified. The coefficients A and B can be calculated by the boundary conditions when i = 1 and 2, as shown in Eq. (18).

$$\omega = \sqrt{\xi^2 + 4\xi} \tag{15}$$

$$\begin{cases} x_1 = \dfrac{2+\xi+\omega}{2} \\ x_2 = \dfrac{2+\xi-\omega}{2} \end{cases} \tag{16}$$

$$s_2 = s_1 + \xi_s s_1 - \xi_c(s_2 + s_3 + \cdots + s_n) = (1+\xi)s_1 - \xi_c \frac{F}{k_p} = (1+\xi)s_1 - d_1^c \tag{17}$$

$$\begin{cases} A = \dfrac{(\omega+\xi)}{2\omega}s_1 - \dfrac{1}{w}d_1^c \\ B = \dfrac{(\omega-\xi)}{2\omega}s_1 + \dfrac{1}{w}d_1^c \end{cases} \tag{18}$$

According to Eqs. (1), (5) and (11), Eq. (19) shows the relationship between the applied load and slips. Further, the slip of the first perfobond connector s_1 can be calculated by substituting the general Eq. (14) into Eq. (19). Finally, all the slip s_i are obtained.

$$F = k_s\left[(1+\xi)s_n - s_{n-1}\right] \tag{19}$$

For the PBL groups with rubber rings, the holes have different shear stiffness. Based on Eqs. (8) and (9), Eq. (11) should be rewritten as the following Eq. (20). By calculating their difference, the simplified relationship between the slips and the stiffness Eq. (21) comes out.

$$s_i + \frac{1}{k_s}\sum_{j=1}^{i} s_j k_{pj} - \frac{1}{k_c}\sum_{j=i+1}^{n} s_j k_{pj} = s_{i+1}, \quad i = 1 \cdots n-1 \tag{20}$$

$$s_{i-2} - [2 + (\frac{1}{k_s} + \frac{1}{k_c})k_{p(i-1)}]s_{i-1} + s_i = 0, \quad i = 3 \cdots n \tag{21}$$

A total of n equations, including the first and last equations in (20) and the n-2 equations of (21), can be used to solve the n unknown slips. The relative slip s_i can be solved by the homogeneous linear Eq. (22). Subsequently, the shear percentages are obtained by normalizing the product of the relative slip s_i, and the corresponding shear stiffness k_{pi}.

$$\begin{bmatrix} 1+\frac{k_{p1}}{k_s} & -1-\frac{k_{p2}}{k_c} & -\frac{k_{p3}}{k_c} & \cdots & \cdots & -\frac{k_{pn}}{k_c} \\ 1 & -2-\frac{k_{p2}}{k_s}-\frac{k_{p2}}{k_c} & 1 & & & \\ & 1 & -2-\frac{k_{p3}}{k_s}-\frac{k_{p3}}{k_c} & 1 & & \\ & & \cdots & \cdots & \cdots & \\ & & & 1 & -2-\frac{k_{pn-1}}{k_s}-\frac{k_{pn-1}}{k_c} & 1 \\ \frac{k_{p1}}{k_s} & \cdots & \cdots & \frac{k_{pn-2}}{k_s} & 1+\frac{k_{pn-1}}{k_s} & -1-\frac{k_{pn}}{k_c} \end{bmatrix} \times \begin{bmatrix} s_1 \\ s_2 \\ \vdots \\ \vdots \\ s_{n-1} \\ s_n \end{bmatrix} = \begin{bmatrix} 0 \\ 0 \\ \vdots \\ \vdots \\ 0 \\ 0 \end{bmatrix} \tag{22}$$

5.2 Stiffness parameters

In the derivation above, the stiffness of PBL, steel plates and concrete blocks are the key parameters. The shear stiffness of PBLs without rubber rings can be calculated through the stiffness equation for a single hole (Eq. (23)) proposed by Zheng (2016), where the shear stiffness was defined as the secant slope at the slip of 0.2 mm on the shear-slip curves. Based on the parametric study (Liu 2019), 6% and 2.5% of the shear stiffness of ordinary PBLs are taken for the holes with 0.5 mm and 1 mm thick rubber rings. The axial stiffness of steel plate and concrete block are expressed as Eq. (24).

$$k_p = (0.27 + 0.14 n_E n_d^2) E_c d \tag{23}$$

$$k_s = \frac{E_s A_{se}}{a_e}, \quad k_c = \frac{E_c A_c}{a_e} \tag{24}$$

$$a_e = a - (\frac{a}{150} - \frac{1}{3})d \tag{25}$$

Where n_E is Young's modulus ratio between perforated rebar and concrete block; n_d is the diameter ratio of perforated rebar to circle hole; E_c and E_s are the elastic moduli of concrete block and steel plate (MPa); d is the hole diameter of perfobond connector (mm); A_{se} is the effective cross-sectional area of steel plates, $A_{se} = t \cdot (w - 0.5 \cdot d)$ (mm^2); A_c is the cross-sectional area of concrete blocks (mm^2); a_e is the effective hole spacing considering the length effect (mm).

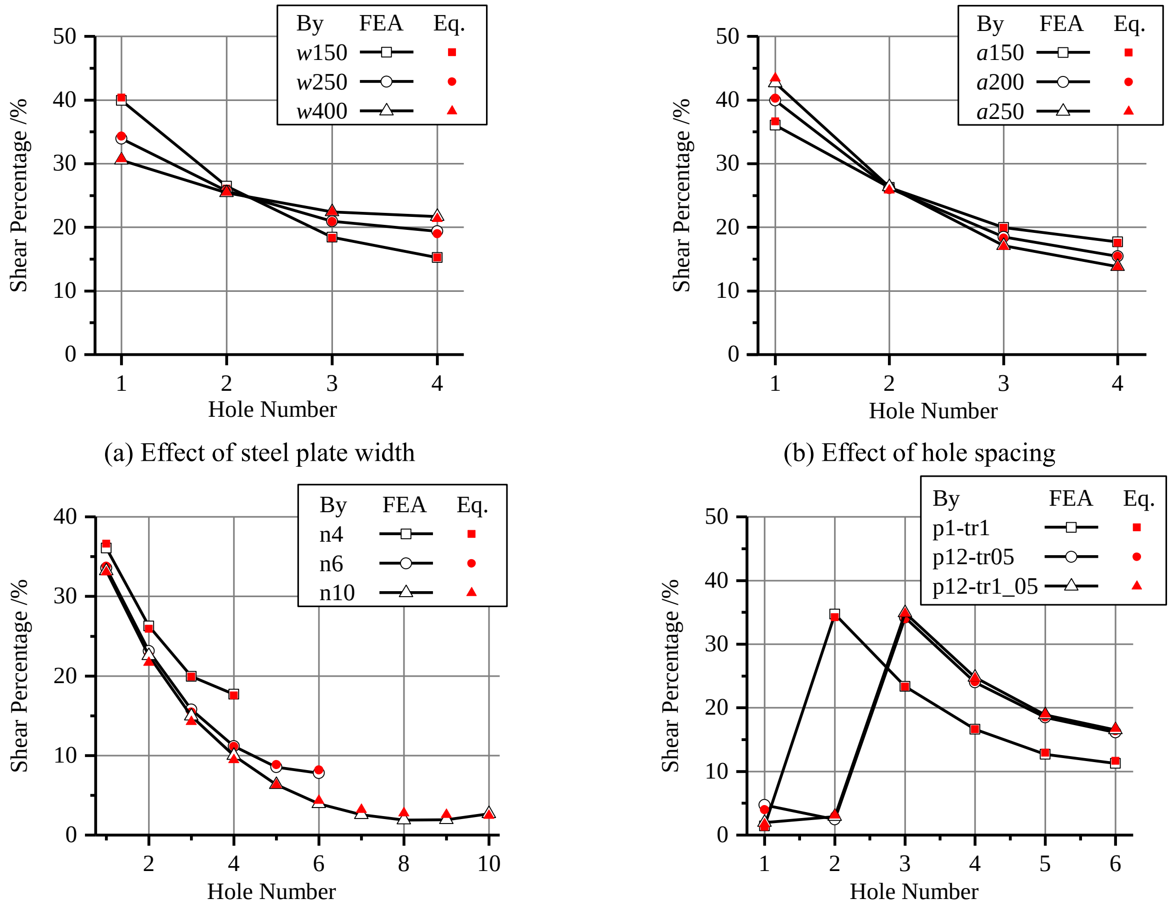

(a) Effect of steel plate width

(b) Effect of hole spacing

(c) Effect of hole number

(d) Effect of rubber ring shemes

Fig. 20 Equations validation by FEA results.

5.3 Equations validation

To verify the theoretical model, the shear distributions of PBLs calculated by the equations in this section are compared with those by the FEA results, as shown in Fig. 20. Since the shear percentages in the FEA models vary with the loading process, the shear percentage is picked at the slip of 0.2 mm (Zheng 2016), which is consistent with the definition of the shear stiffness in Eq. (23). The x-axis in the figures is the hole number from top to bottom. The comparisons show that the theoretical and numerical results are in good agreement under the varying steel plate widths, hole spacings and the numbers of holes. The proposed equations are feasible to evaluate the shear distribution of PBL groups with identical or different shear stiffness in the serviceability stage.

6. Conclusions

This paper presents the modified push-out tests for five specimens with multi-row PBLs to investigate the effects of rubber rings on the shear mechanism of PBL groups. The 3-D refined FE models were established and validated by the test results. Furthermore, the effects of the width of steel plates, spacing and numbers of holes, rubber ring thicknesses, and positions of rubber rings on the shear distribution were investigated by the parametric study. Finally, an analytical model for PBL groups allowing that the connectors have different stiffness was proposed to predict the shear distribution at the serviceability stage. The following conclusions could be addressed:

- Employing rubber rings on partial holes can increase the slip ability of PBL groups. According to the strain difference of perfobond plates between the first two rows and the longitudinal strains of perforated rebars, rubber rings can postpone the shear resistance of partial holes in PBL groups.
- The numerical results show that the shear strength of holes in the middle rows is fully exerted by using rubber rings on the top and bottom holes. When the concrete block has relatively large dimensions, setting a rubber ring on the bottom hole is unnecessary. The reasonable thicknesses of rubber rings are 1 mm and 0.5 mm in practice.
- Based on the parametric study, the unevenness of shear forces decreases by reducing the stiffness ratio of PBLs to perfobond plates and the number of holes. When the shear stiffness of holes with rubber rings recover, the shear percentages of the holes without

rubber rings drop rapidly, indicating the shear forces redistribute in the PBL group. Reasonable rubber ring schemes can improve the composite behavior of PBL groups.

- An analytical model for PBL groups allowing that the connectors have different stiffness is proposed. Furthermore, the shear force distribution equation of perfobond connectors at the serviceability stage is derived, which agrees well with the numerical results.

References

ABAQUS Documentation. Version 6.12. (2012), Dassault system, USA.

Ahn, J.H., *et al.* (2010), "Shear resistance of the perfobond-rib shear connector depending on concrete strength and rib arrangement", *J. Constr. Steel Res.*, **66**(10), 1295-1307. https://doi.org/10.1016/j.jcsr.2010.04.008.

Al-Darzi, S.Y.K., Chen, A.R. and Liu, Y.Q. (2007), "Finite element simulation and parametric studies of perfobond rib connector", *Am. J. Appl. Sci.*, **4**(3), 122-127.

Allahyari, H., Dehestani, M., Beygi, M.H., Neya, B.N. and Rahmani, E. (2014), "Mechanical behavior of steel-concrete composite decks with perfobond shear connectors", *Steel Compos. Struct.*, **17**(3), 339-358. http://dx.doi.org/10.12989/scs.2014.17.3.339.

Cândido-Martins, J.P.S., Costa-Neves, L.F. and Vellasco, P.D.S. (2010), "Experimental evaluation of the structural response of Perfobond shear connectors", *Eng. Struct.*, **32**(8), 1976-1985. https://doi.org/10.1016/j.engstruct.2010.02.031.

CEB-FIP Model Code 2010, (2010), British Standard Institution.

Classen, M. and Hegger, J. (2017), "Shear-slip behaviour and ductility of composite dowel connectors with pry-out failure", *Eng. Struct.*, **50,** 428-437. https://doi.org/10.1016/j.engstruct.2017.07.065.

Classen, M. (2018), "Limitations on the use of partial shear connection in composite beams with steel T-sections and uniformly spaced rib shear connectors", *J. Constr. Steel Res.*, **142**, 99-112. https://doi.org/10.1016/j.jcsr.2017.11.023.

EUROCODE 4, EN 1994-1-1, (2005), Design of Composite Steel and Concrete Structures Part 1.1 General Rules and Rules for Buildings, CEN-European Committee for Standardization, Brussels.

Hechler, O., Berthellemy, J., Lorenc, W., Seidl, G. and Viefhues, E. (2011), Continuous shear connectors in bridge construction. In Composite Construction in Steel and Concrete VI (pp. 78-91).

Khorramian, K., Maleki, S., Shariati, M., Jalali, A. and Tahir, M.M. (2017), "Numerical analysis of tilted angle shear connectors in steel-concrete composite systems", *Steel Compos. Struct.*, **23**(1), 67-85. https://doi.org/10.12989/scs.2017.23.1.067.

Kim, K.S., Han, O., Gombosuren, M. and Kim, S.H. (2019), "Numerical simulation of Y-type perfobond rib shear connectors using finite element analysis", *Steel Compos. Struct.*, **31**(1), 53-67. https://doi.org/10.12989/scs.2019.31.1.053.

Kim, S.H., Lee, C.G., Ahn, J.H. and Won, J.H. (2011), "Experimental study on joint of spliced steel–PSC hybrid girder, Part I: Proposed parallel-perfobond-rib-type joint", *Eng. Struct.*, **33**(8), 2382-2397. https://doi.org/10.1016/j.engstruct.2011.04.012.

Kraus, D. and Wurzer, O. (1997), "Nonlinear finite-element analysis of concrete dowels", *Comput. Struct.*, **64**(5-6), 1271-1279. https://doi.org/10.1016/S0045-7949(97)00034-5.

Liu, Y., Xin, H. and Liu, Y. (2018), "Load transfer mechanism and fatigue performance evaluation of suspender-girder composite anchorage joints at serviceability stage", *J. Constr. Steel Res.*, **145**, 82-96. https://doi.org/10.1016/j.jcsr.2018.02.010.

Liu, Y., Xin, H. and Liu, Y. (2019), "Experimental and analytical study on shear mechanism of rubber-ring perfobond connector", *Eng. Struct.*, **197**, 109382. https://doi.org/10.1016/j.engstruct.2019.109382.

Nguyen, H.T. and Kim, S.E. (2009), "Finite element modeling of push-out tests for large stud shear connectors", *J. Constr. Steel Res.*, **65**(10-11), 1909-1920. https://doi.org/10.1016/j.jcsr.2009.06.010.

Oguejiofor, E.C. and Hosain, M.U. (1994), "A parametric study of perfobond rib shear connectors", *Can. J. Civil Eng.*, **21**(4), 614-625. https://doi.org/10.1139/l94-063.

Pavlović, M., Marković, Z., Veljković, M. and Buđevac, D. (2013), "Bolted shear connectors vs. headed studs behaviour in push-out tests", *J. Constr. Steel Res.*, **88**, 134-149. https://doi.org/10.1016/j.jcsr.2013.05.003.

Spremic, M., Pavlovic, M., Markovic, Z., Veljkovic, M. and Budjevac, D. (2018), "FE validation of the equivalent diameter calculation model for grouped headed studs", *Steel Compos. Struct.*, **26**(3), 375-386. https://doi.org/10.12989/scs.2018.26.3.375.

Zheng, S., *et al.* (2016), "Parametric study on shear capacity of circular-hole and long-hole perfobond shear connector", *J. Constr. Steel Res.*, **117**, 64-80. https://doi.org/10.1016/j.jcsr.2015.09.012.

BU